Geomechanics and Engineering, *Vol. 25, No. 1 (2021) 31-40*
DOI: https://doi.org/10.12989/gae.2021.25.1.031

Evaluation of Injection capabilities of a biopolymer-based grout material

Minhyeong Lee[1a], Jooyoung Im[1b], Ilhan Chang[2c] and Gye-Chun Cho[*1]

[1]*Department of Civil and Environmental Engineering, Korea Advanced Institute of Science and Technology, 291 Daehak-ro, Yuseong-gu, Daejeon 34141, Republic of Korea*
[2]*Department of Civil Systems Engineering, Ajou University, 206 World cup-ro, Yeongtong-gu, Suwon-si 16499, Gyeonggi-do, Republic of Korea*

(Received January 11, 2021, Revised February 18, 2021, Accepted February 19, 2021)

Abstract. Injection grouting is one of the most common ground improvement practice to increase the strength and reduce the hydraulic conductivity of soils. Owing to the environmental concerns of conventional grout materials, such as cement-based or silicate-based materials, bio-inspired biogeotechnical approaches are considered to be new sustainable and environmentally friendly ground improvement methods. Biopolymers, which are excretory products from living organisms, have been shown to significantly reduce the hydraulic conductivity via pore-clogging and increase the strength of soils. To study the practical application of biopolymers for seepage and ground water control, in this study, we explored the injection capabilities of biopolymer-based grout materials in both linear aperture and particulate media (i.e., sand and glassbeads) considering different injection pressures, biopolymer concentrations, and flow channel geometries. The hydraulic conductivity control of a biopolymer-based grout material was evaluated after injection into sandy soil under confined boundary conditions. The results showed that the performance of xanthan gum injection was mainly affected by the injection pressure and pore geometry (e.g., porosity) inside the soil. Additionally, with an increase in the xanthan gum concentration, the injection efficiency diminished while the hydraulic conductivity reduction efficiency enhanced significantly. The results of this study provide the potential capabilities of injection grouting to be performed with biopolymer-based materials for field application.

Keywords: biopolymer; injection grouting; hydrogel; penetrability; hydraulic conductivity

1. Introduction

In ground improvement practice, injection grouting is generally performed by injecting chemical compounds (e.g., cement, lime, bentonite, and waterglass-based chemicals) into the ground or water-retaining structures (e.g., levee, dam, and embankment) with a sufficient pressure gradient to strengthen the soil and reduce its hydraulic conductivity (Eklund and Stille 2008).

Previous studies on grout materials have mainly focused on the grouting performance and engineering capabilities of grouted granular soil using cement-based or clay slurry-based grout materials (Akbulut and Saglamer 2002, Santagata and Santagata 2003). The groutability of soils is commonly defined as the ability of a grout material to permeate through the soil media. As most existing grout materials are particle dispersed fluids (e.g., cement-based or clay slurries), groutability is assessed based on the relative grain size ratio between the soil and grout material (i.e., $D_{15,soil}/d_{85,grout}$) (Burwell 1958, Bell 1993). In addition, the apparent viscosity and rheological properties become important considerations for clay-based slurry grout (e.g., bentonite) (Yoon and El Mohtar 2014).

However, common grouting materials (e.g., cement and lime) have been shown to cause large greenhouse gas emissions and to have a strong chemical impact on the environment (Benhelal *et al.* 2013). Therefore, biological materials and methods are actively being introduced to geotechnical engineering as environmentally friendly alternatives (Whiffin *et al.* 2007, DeJong *et al.* 2010, Jeon *et al.* 2017, Chang *et al.* 2019, Kim *et al.* 2019).

Among these environmentally friendly methods, biopolymer-based soil treatment (BPST) has been shown to significantly enhance the geotechnical properties of soil (Chang *et al.* 2016, Choi *et al.* 2020). Furthermore, BPST methods have been shown to induce strengthening (Chang and Cho 2012, Chang *et al.* 2015, Chang *et al.* 2015, Qureshi *et al.* 2017, Ham *et al.* 2018, Lee *et al.* 2019, Kwon *et al.* 2020, Soldo *et al.* 2020), permeability reduction (Bouazza *et al.* 2009, Chang *et al.* 2016, Noh *et al.* 2016), and plant growth promotion (Larson *et al.* 2010, Chang *et al.* 2015, Tran *et al.* 2019) in laboratory-scale assessments and field application trials (Ko and Kang 2018, Chang *et al.* 2020).

Considering the beneficial effect of the BPST on the hydraulic conductivity reduction in soils, it has high potential for seepage and infiltration control. However, further studies are required for the implementation of the BPST method. In particular, it is essential to understand the

∗Corresponding author, Professor
E-mail: gyechun@kaist.edu
[a]Ph.D. Student
E-mail: minhyeong@kaist.ac.kr
[b]Post-Doctoral Researcher
E-mail: jooyoungim@kaist.ac.kr
[c]Associate Professor
E-mail: ilhanchang@ajou.ac.kr

ISSN: 2005-307X (Print), 2092-6219 (Online)

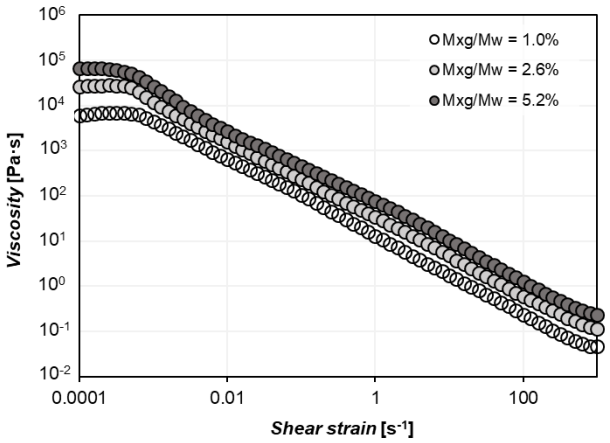

Fig 1 Reduction of XG viscosity with increasing shear strain

injection performance of biopolymers into soils.

In this study, the injection behavior of xanthan gum (XG) biopolymer has been assessed to verify its technical feasibility to become a new grout material. XG hydrogel well known for its shear-thinning characteristic, where the viscosity reduces with shear rate increase as shown in Fig 1 (Zhong *et al.* 2013, Lee *et al.* 2021), while the reduced viscosity recovers when the applied strain is removed (Sworn 2021). Such properties have allowed the utilization of XG hydrogels in various medical applications as injectable biomaterial in vivo (Liu and Yao 2015).

To verify the injection effectiveness of XG hydrogel as a new geotechnical grouting material, two types of laboratory injection tests were carried out in this study: 1) linear injection into a constraint uniform aperture and 2) injection into a particulate media. In the linear injection tests, XG hydrogel was injected into a quantified aperture under different injection pressures and biopolymer concentrations. The injection test in a particulate media (i.e., sand and glassbeads) were evaluated in lab-scale experimental tests in which a simplified injection grout was performed in confined granulated particles. Additionally, the hydraulic conductivity was measured after that XG hydrogel fully injected into the particulate media. The injection efficiency and hydraulic conductivity reduction capabilities of the BPST soils analyzed in this study provide fundamental insights into the potential of biopolymer-based grouting.

2. Materials and methods

2.1 Materials

2.1.1 Biopolymers: Xanthan gum (XG)

Xanthan gum (Sigma–Aldrich®, CAS number 11138-66-2) was used as the main biopolymer. XG is a polysaccharide biopolymer widely used as a food additive. It has pseudo plastic characteristics and can greatly increase the viscosity of a fluid (Casas *et al.* 2000, García-Ochoa *et al.* 2000). Because an increasing biopolymer concentration results in an increasing fluid viscosity, the effects of injection will be highly dependent on the biopolymer

Table 1 Index properties of tested particulate materials

Properties	Jumunjin sand	GB1	GB2	GB3
D_{50} [mm]	0.47	0.74	1.59	2.65
G_s	2.65	2.48	2.48	2.48
C_u	1.12	1.40	1.33	1.32
C_c	0.98	1.05	0.96	0.95
e_{max}	0.95	0.69	0.69	0.69
e_{min}	0.64	0.55	0.55	0.55

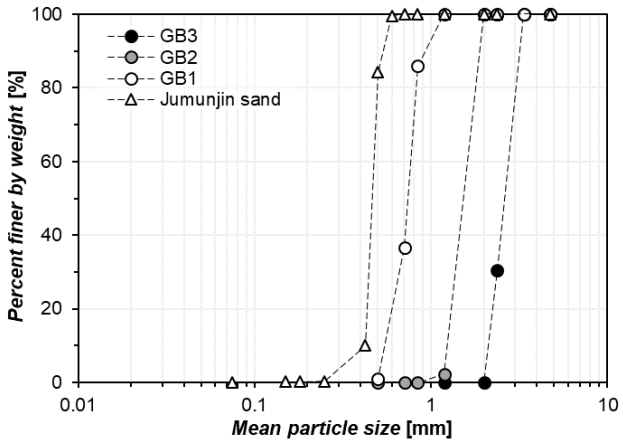

Fig 2 Particle size distribution of Jumunjin sand and glassbeads

concentration. In this study, XG hydrogel is prepared for 1.25%, 2.5%, and 5.0% concentration (i.e. ratio of XG powder weight to water weight, M_{XG}/M_W).

2.1.2 Particulate material: sand and glassbeads

Jumunjin sand and glassbeads with three different sizes were used as representative particulate materials (Fig. 2). Jumunjin sand, which has a USCS classification as a poorly graded sand (*SP*), has a mean particle size (D_{50}) of 0.47 mm, coefficient of uniformity (C_u) of 1.12, and coefficient of curvature (C_c) of 0.98. Its maximum and minimum void ratio (e_{max} and e_{min}, respectively) are 0.95 and 0.64, respectively.

Glassbeads with three different sizes were prepared to consider the effects of the pore dimension on the injectability of XG hydrogel. Glassbeads were purchased from B&K MEDIA Co, Ltd., in South Korea. In this study, spherical glassbeads with D_{50} of 0.74, 1.59, and 2.65 mm were used and denoted as GB1, GB2, and GB3, respectively. The properties of Jumunjin sand and glassbeads are summarized in Table 1.

2.2 Experimental programs

2.2.1 Xanthan gum (XG) hydrogel preparation

To prepare a XG-based injection solution, XG powder was uniformly dissolved in distilled water at room temperature (21°C) using a magnetic stirrer until a uniform hydrogel was achieved. The XG mass to water mass ratio (M_{XG}/M_W) was set to 0.5%, 1.0%, and 2.0% for the parallel plate injection test and to 1.25%, 2.5%, and 5.0% for the particulate media injection test.

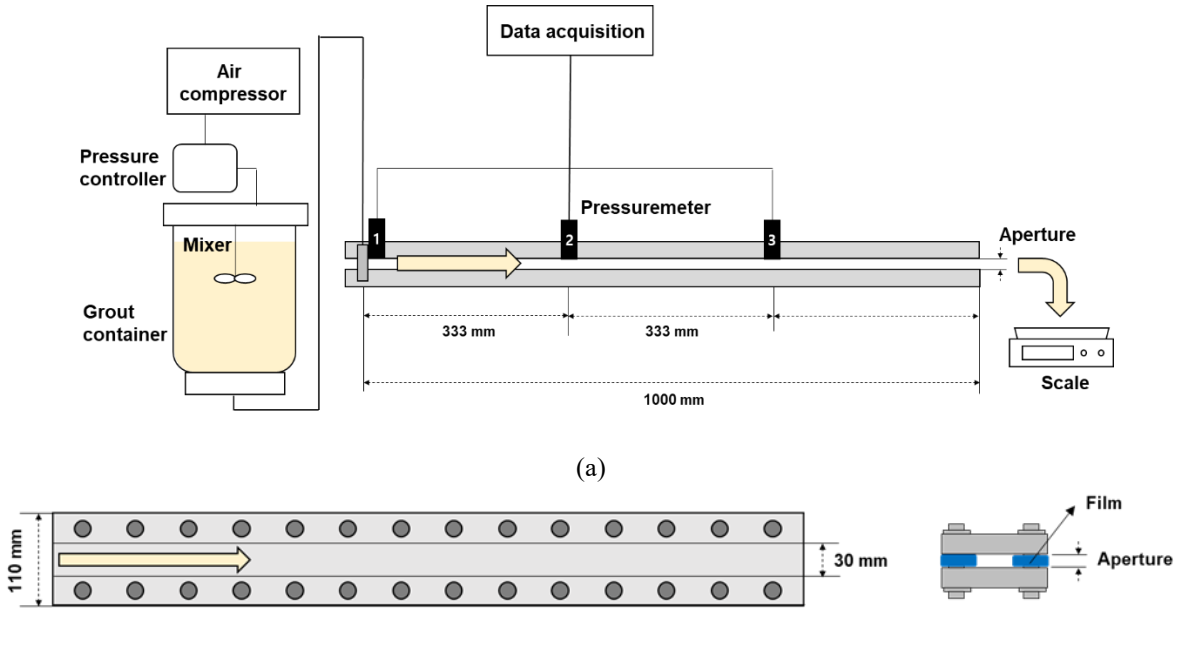

Fig. 3 Schematic of (a) experimental setup, and (b) plane view and cross-section of parallel plate

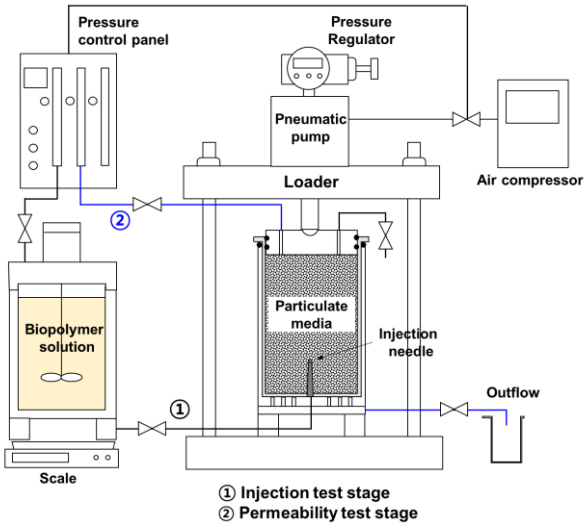

Fig. 4 Schematic of injection into particulate media and permeability evaluation setup

2.2.2 Parallel plate (Linear flow) grout injection test

The parallel plate grout injection apparatus is designed to evaluate the flow passage and spread performance of a grout material injected into an uniform aperture geometry which represents micro cracks of geomaterials (e.g., jointed rock) (Jin *et al.* 2016). This equipment is used to measure the flow rate with the discharge volume of the injection material being transported in one direction through quantified apertures.

The experimental setup consists of a pressure supply system (i.e., air compressor), grout material container, parallel plate including pressure meters, and data acquisition system (Fig. 3(a)). Two (i.e., top and bottom) rectangular stainless-steel plates with a thickness of 15 mm, width of 110 mm, and length of 1000 mm were aligned parallelly with different spacings as 0.25, 0.5, and 0.75 mm. A polyester industrial film with a heat shrinkage below 1% and an elastic coefficient of 4.4 GPa was installed with various thicknesses to regulate the width of apertures between the top and bottom plates (Fig. 3(b)). Grout materials were prepared in a grout container; the cap of the chamber has a pressure controller to maintain the applied air pressure in the chamber. Three pressure meters were installed on the top plate in order to monitor the injection process of the grout material.

The grout material flowed in one-dimension through an aperture with a width of 30 mm, and the passage time, final flow rate, and steady state pressure applied at each

Table 2 Detailed condition of grout injection test into particulate media

Experiment	Injection process				Injection process and Constant head permeability test		
Case #	1	2	3	4	5	6	7
Material	GB3	GB2	GB1	Sand	Sand	Sand	Sand
D_{50} [mm]	2.65	1.59	0.74	0.47	0.47	0.47	0.47
Dry density (ρ_d) [g/cm^3]	1.52	1.53	1.53	1.49	1.50	1.51	1.50
Void ratio (e)	0.61	0.61	0.60	0.77	0.76	0.75	0.77
Porosity (n)	0.38	0.39	0.37	0.43	0.42	0.43	0.43
Relative density (D_r) [%]	59	59	65	58	61	64	60
Injection pressure [kPa]	100	100	100	100	300	300	300
M_{XG}/M_W [%]	2.5	2.5	2.5	2.5	1.25	2.5	5.0

monitoring point can be measured over time. Xanthan solution with an M_{XG}/M_W of 0.5%, 1.0%, and 2.0% was injected into apertures under three different injection pressures (200, 400, and 600 kPa).

2.2.3 Grout injection test into particulate media and hydraulic conductivity evaluation

The setup for the injection process was designed to simulate XG hydrogel injection into a particulate media in a cylinder form with diameter and height of 100 and 200 mm, respectively. A truncated cone-shaped injection needle with a volume of 5.1 cm^3 was inserted at the bottom of the specimen. Firstly, XG solution and particulate media were prepared in the XG hydrogel chamber and specimen cell, respectively. The particulate media (i.e., dry sand or glassbeads) was filled inside the cell and compacted via tamping three continuous layers to represent a consistent initial density condition. Then the medium in the cell was saturated by deionized water with the outlet valve at the cell bottom part being closed. The confining cap was placed on the top and excess water in the saturated cell was drained through the valve on the cap.

After the preparation of the specimen, a vertical confining stress was applied on the drained specimen by a pneumatic loader (GCTS FRM-010C) with a pressure of 400 kPa to prevent the volume expansion of particles during injection. Then, constant pneumatic pressure (i.e., 100, 300 kPa) was applied into the XG hydrogel chamber through the cap valve to inject XG hydrogel into the specimen cell via the injection needle. During the injection process, the weight decrease of the XG hydrogel chamber was measured to quantify the amount of hydrogel injected, and the injected volume was estimated using an empirically estimated density (0.53 cm^3 per unit gram) of the XG hydrogel in the pore spaces of the soil. Then, this value was used to estimate when XG hydrogel injection was completed, after which the valve connected to the biopolymer chamber was closed.

Following the injection, a water inflow with a constant hydraulic head was supplied through the top cap valve of the specimen to measure the hydraulic conductivity of the grouted sample according to ASTM 2434-19 (ASTM 2019). Since XG hydrogel generally remains stable under wet (moisture-maintained) condition without strain (e.g., hydrogel flow), the effect post-injection curing time is expected to be less significant, thus, the curing time was not considered as major factor in this study.

The injection process was carried out in seven different attempts as listed in Table 2. In cases 1-4, the glassbead and sand specimens were subjected to XG injection at 100 kPa, and the effects of the pore size on the injectability of the XG solution were considered. On the other hand, both the injection process and the hydraulic conductivity tests were performed on the sand specimens (cases 5-7) in order to examine the impact of the XG hydrogel concentration on the injection capabilities and hydraulic conductivity of the soil.

2.2.4 Environmental scanning electron microscopy analysis of xanthan gum (XG)

Environmental scanning electron microscope (ESEM) is able to observe materials in a dynamic in-situ environment unlike conventional SEM analysis. In particular, micro analysis becomes possible with various humid conditions by adjusting the vapor pressure in the chamber. In this study, pure xanthan gum powder was observed by ESEM (Thermo Fisher Scientific, Quattro S) under different humidity conditions to identify the behavior of XG hydrogel in pore structure. As increasing the vapor pressure from 51 kPa to 730 kPa, the expansion behavior of dried XG powder under humidity increment was observed.

3. Results and analysis

3.1 Injection performance of XG hydrogel in linear flow

Fig. 5 shows the flow rate of XG hydrogel assessed by the parallel plate injection test. As expected, a higher XG concentration leads to a lower one-dimensional flow rate. Despite the overall behavior of the flow rate shows a linear response to the increase in the injection pressure, the injection pressure becomes more predominant when the XG concentration decreases. From these linear trends, the minimum required injection pressure based on the XG concentration and pore spacing were estimated, and the results are summarized in Table 3. At the smallest aperture size of 0.25 mm, the estimated minimum required pressure was obtained to be approximately 158-218 kPa depending on the M_{XG}/M_W.

In the case of the parallel plate linear flow test, the behavior of the fluid flow through the plates was found to be in accordance with that in the laminar flow conditions. To estimate the theoretical fluid flow rate of the XG solution, the viscosity values at different XG concentrations were determined using the Poiseuille equation as

$$\Delta p = \frac{8\pi\mu LQ}{A^2} \quad (1)$$

where Δp is pressure gradient (Pa), μ is viscosity (Pa·s), L is flow length (m), Q is flow rate (m^3/s), and A is cross-sectional area (m^2).

Table 3 Flow rate of xanthan gum hydrogel obtained via parallel plate grout injection test

M_{XG}/M_W [%]	Aperture size [mm]								
	0.25			0.50			0.75		
	Applied pressure [kPa]	Flow rate [cm³/min]	Minimum required pressure [kPa]	Applied pressure [kPa]	Flow rate [cm³/min]	Minimum required pressure [kPa]	Applied pressure [kPa]	Flow rate [cm³/min]	Minimum required pressure [kPa]
0.5	200	13.9	158.5	200	72.3	155.1	200	899.6	47.2
	400	76.4		400	524.1		400	2214.7	
	600	142.4		600	871.5		600	3704.5	
1.0	200	3.2	177.2	200	23.5	174.1	200	162.5	82.6
	400	46.4		400	257.9		400	720.1	
	600	81.9		600	462.7		600	1571.5	
2.0	200	0.5	218.8	200	7.6	187.5	200	87.2	181.2
	400	2.6		400	91.5		400	272.2	
	600	10.3		600	187.1		600	784.3	

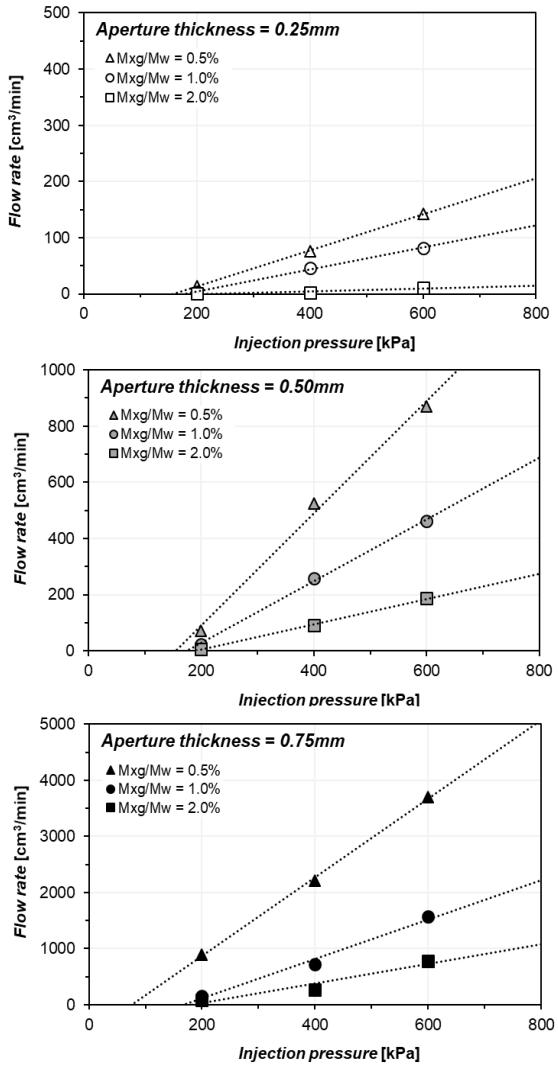

Fig. 5 Flow rate in one-dimensional flow of xanthan gum hydrogels under injection pressure and aperture size

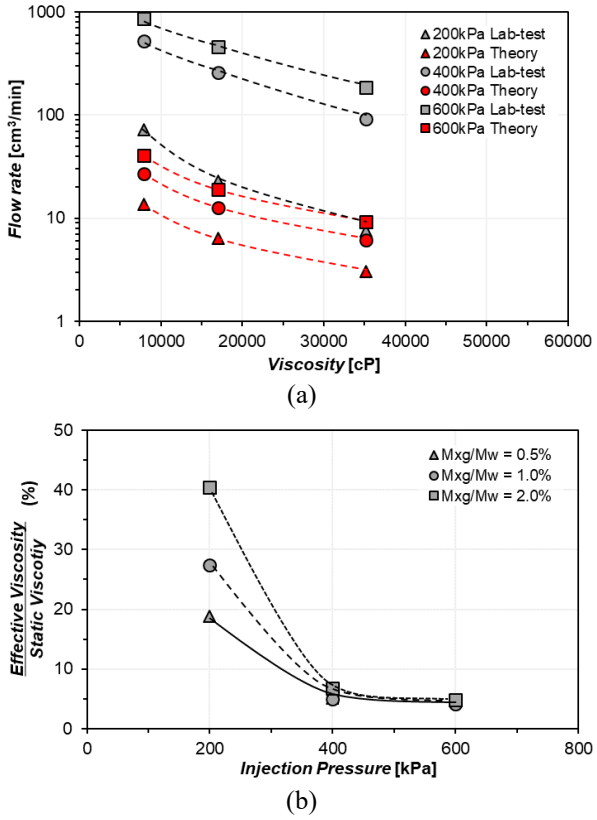

Fig. 6 Linear injection estimations at aperture thickness of 0.5 mm: (a) Experimental and theoretic flow rates and (b) Effect of injection pressure on the viscosity reduction of XG

The viscosity values obtained are shown in Fig. 6(a). From the figure, it can be seen that the theoretic flow rate of the XG solution, was significantly lower than the experimental fluid flow rate. The theoretical flow rate is obtained based on the viscosity of XG hydrogels at rest (i.e. low strain rate), while XG is shear-thinning material which viscosity decreases with strain rate increase. Thus, the higher injection flow rate assessed in lab-tests can be postulated as an attribution of the shear-thinning of XG.

In addition, higher injection pressure also seems to have an impact on XG solution viscosity reduction and following

Table 4 Injection performance by particle size

Cases	1	2	3	4
Injection rate for initial 10 s [cm^3/min]	507	312	42	18
Injection rate for initial 60 s [cm^3/min]	311	138	35	13
Final injection rate [cm^3/min]	38	10	1.2	0.01
Total injection time [s]	65	340	3600	32400

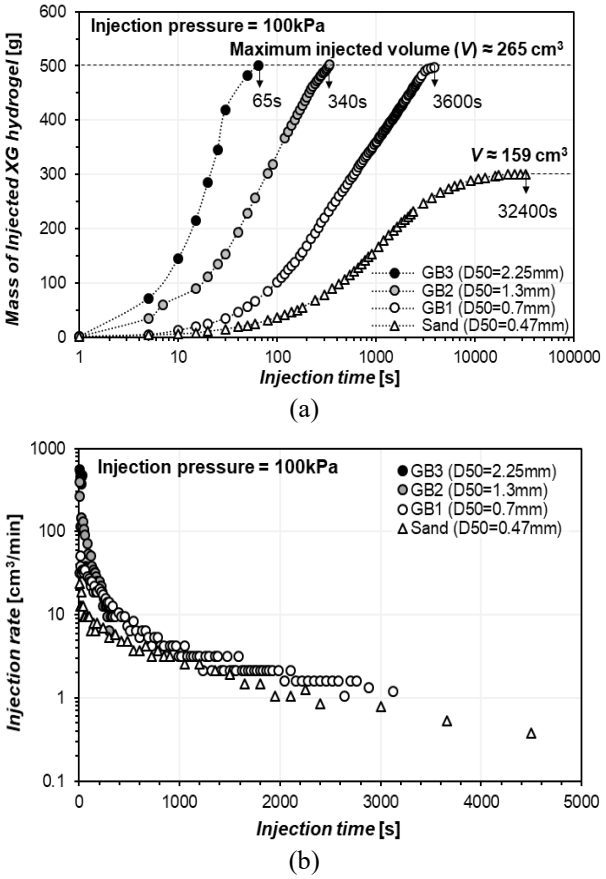

Fig. 7 Injection of XG hydrogel (M_{XG}/M_W = 2.5%) into different particulate media at 100 kPa. (a) Mass of injected XG solution and (b) Injection rate variation

flow rate increase. The degree of viscosity reduction can be observed from the experimental flow results (Fig. 6(b)).

The results show that at injection pressures above 400 kPa, the effective viscosity of the solution converges to approximately 5% of the static viscosity. These results indicate that higher pressure gradients will increase the penetration efficiency in which XG can be injected into a medium.

3.2 Injection performance of xanthan gum (XG) in particulate-porous media

Fig. 7 and Table 4 present the results of the XG injection into glassbeads and sand at an injection pressure of 100 kPa (cases 1-4). The time required to inject the XG hydrogel throughout the GB3, GB2, and GB1 specimens (approximately 500 g and 265 cm^3) was 65, 340, and 3600 seconds, respectively. As expected, the XG hydrogel injection rate was shown to increase with an increase in the diameter of the glassbead (Fig. 7). However, in the case of sand, the injected volume of XG hydrogel tended to level off as injection progressed. It was noted that an injection pressure of 100 kPa was insufficient for XG injection into the entire sand specimen.

This result indicates that it is insufficient to inject viscous XG hydrogel with an injection pressure of 100 kPa.

Table 5 Estimated pore diameter of particulate material used in this study

				Simple cubic[1] (n = 0.48)	Orthorhombic[1] (n = 0.40)	Tetrahedral[1] (n = 0.26)	Closed-packed[2] ($n \approx 0.4$)
				$0.73D_{50}$	$0.53D_{50}$	$0.41D_{50}$	$0.33D_{50}$–$0.1D_{50}$
Cases	Material	D_{50} [mm]	Porosity (n)	Estimated pore diameter by spherical glassbead packing [mm]			
1	GB3	2.65	0.38	1.94	1.41	1.10	0.27-0.88
2	GB2	1.59	0.39	1.16	0.84	0.66	0.16-0.53
3	GB1	0.74	0.37	0.54	0.39	0.31	0.07-0.25
4	SAND	0.47	0.43	0.34	0.25	0.19	0.05-0.16

[1] Gupta and Larson *et al.* (1979)

[2] Dremin *et al.* (1995)

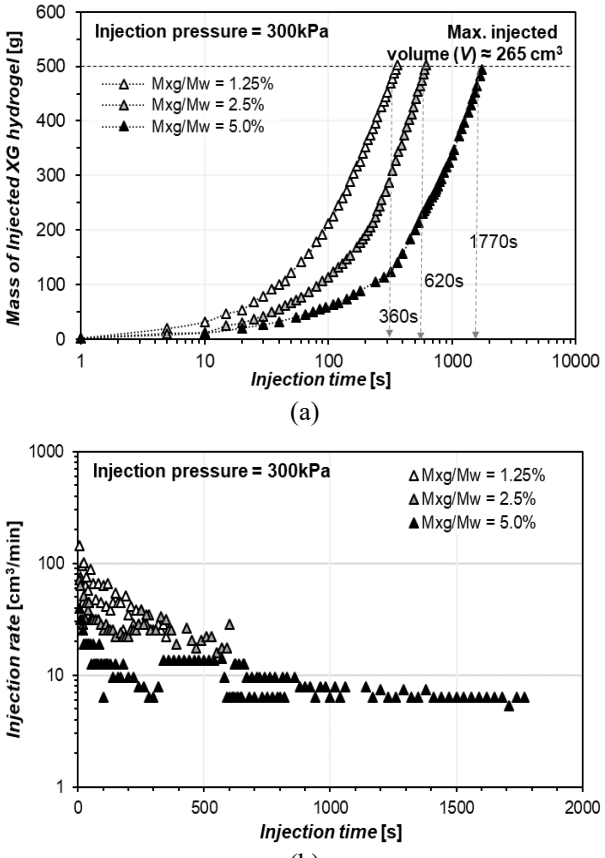

Fig. 8 Injection of different concentrations of XG hydrogel into sand at 300 kPa: (a) mass of injected XG solution and (b) injection rate variation

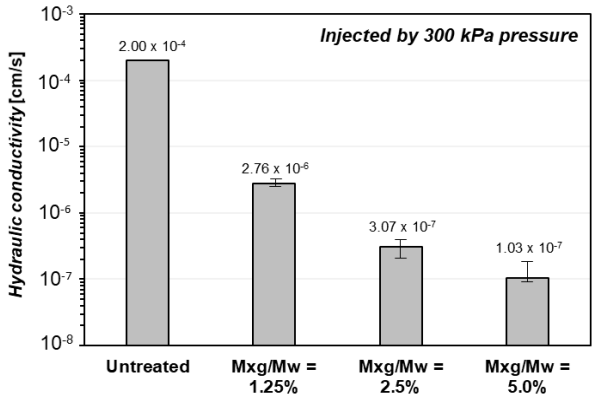

Fig. 9 Hydraulic conductivity of XG hydrogel injected sand

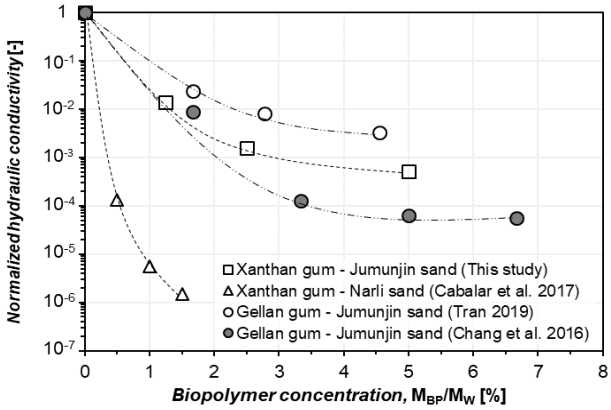

Fig. 10 Normalized hydraulic conductivity of biopolymer hydrogel treated soil

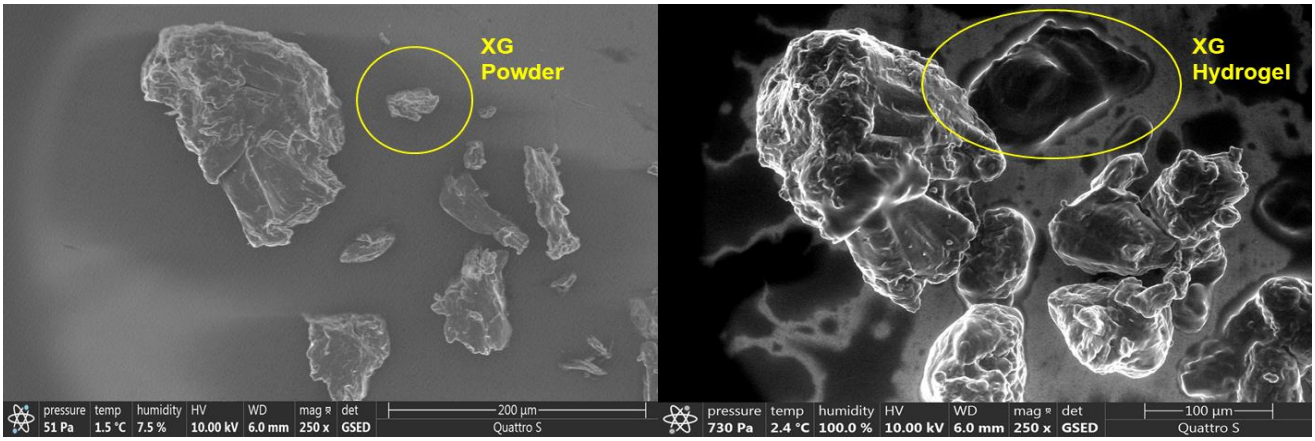

Fig. 11 ESEM images of XG powder in dried state (relative humidity=7.5%) and wet state (relative humidity=100%)

Under similar porosity conditions, a smaller media particle size lead to a smaller equivalent pore diameter through which the fluid passes and a larger exposed surface area of particles (Santamarina *et al.* 2001). Additionally, the increase in the viscosity of the hydrogel could be prevented by the dragging force acting on the particle surface; this effect is estimated to be amplified as the XG hydrogel passes through the smaller pores.

Although it is difficult to quantitatively determine the exact pore diameter of the particulate media prepared in this study, Gupta and Larson (1979) theoretically estimated the representative pore diameter in three packing states of spherical glassbeads to be $0.73D_{50}$, $0.53D_{50}$, and $0.41D_{50}$ for simple cubic, orthorhombic, and tetrahedral packing, respectively. Moreover, Lee *et al.* (1995) suggested that the average pore diameter of glassbeads in a closed-pack (n=0.4) state is within the range of 1/3 to 1/10 of D_{50}. Table 5 presents the pore diameter of the specimens prepared in this study estimated based on these previous studies.

Fig. 8 shows the results of the injection process of XG hydrogel into sand with a 300 kPa pressure (cases 5-7), and Table 6 lists the injection rates at the initial and final stages. It can be seen that when M_{XG}/M_W is 2.5%, the injection rate in the initial 10 s at 300 kPa (case 5) was three times greater

Table 6 Injection performance and hydraulic conductivity control by M_{XG}/M_W

Case	5	6	7
Injection rate for initial 10 s [cm^3/min]	106	67	35
Injection rate for initial 60 s [cm^3/min]	76	41	23
Final injection rate [cm^3/min]	25	13	6
Total Injection time [s]	360	620	1770
k [cm/s]	2.8×10^{-6}	3.1×10^{-7}	1.0×10^{-7}
k/k_o [1] [-]	1.4×10^{-2}	1.5×10^{-3}	5.2×10^{-4}

[1] Hydraulic conductivity of clean sand (k_o)= 2.0×10^{-4} cm/s

than that at 100 kPa (case 4). Meanwhile, as the M_{XG}/M_W increased from 1.25% to 5%, the total time spent for the specimen to be fully injected increased from 360 to 1,770 seconds

In cases 5-7, constant head permeability tests were performed to verify the performance of the injected XG grout on the hydraulic conductivity. Fig. 9 shows the hydraulic conductivity reduction of sand with an increase in the concentration of the injected XG hydrogel. Results show that the hydraulic conductivity decreases exponentially with the injection of XG from 2.0×10^{-4} cm/s (untreated condition) to 1.03×10^{-7} cm/s (M_{XG}/M_W = 5% XG grout). This reduction is expected to be associated with the water holding capacity and pore-filling properties of the XG biopolymer hydrogel. The XG that is injected in to the pore spaces of the sand particles forms a viscous fluid by absorbing the surrounding free water to create a highly viscous hydrogel. Higher concentrations of XG will reduce the available free water within the sand pores thereby further reducing the hydraulic conductivity of the soil. Fig. 10 shows the normalized permeability reduction of XG grout injected sand (this study) plotted with data from previous studies (Chang *et al.* 2016, Cabalar *et al.* 2017, Tran 2019). The bioclogging efficiencies from other studies have shown converging trends towards a lower bound, which indicates that higher concentrations of XG biopolymer have diminishing returns in reducing the hydraulic conductivity of the soil. Thus the hydraulic conductivity is expected to converge towards certain value as M_{XG}/M_W increases above 5%.

3.4 XG swelling observations with ESEM

Fig. 11 presents ESEM images of XG in the dried state (relative humidity = 7.5%) and wet state (relative humidity = 100%). Because XG is hydrophilic, owing to the presence of –OH and –COOH groups in its molecular structure, the water molecules are readily hydrated, resulting in the swelling of XG molecules. As a result, as the relative humidity in the ESEM chamber increases, the XG powder absorbs surrounding water molecules and shows remarkable volume expansion. This indicates that the expansion in the hydrated condition along with the high viscosity result in a pore clogging effect within the soil pores, thereby reducing the hydraulic conductivity.

4. Discussions

4.1 Injection capability and pore clogging effect of XG hydrogel related to shear thinning properties of XG

The XG solution does not contain particles that can affect the injectability of the grout material, so the injection capabilities are mainly dominated by the rheologic viscosity of the solution. The linear injection tests indicated that although higher concentrations of XG resulted in higher viscosities and lower flow rate, the injection of the XG solution becomes easier with higher injection pressures owing to the shear thinning properties of XG.

Furthermore, because the viscosity of XG decreases at higher injection pressures, higher hydraulic gradients within the soil may also lead to a reduction in the XG viscosity and thereby an increase in the hydraulic conductivity. This increase in the hydraulic conductivity may reduce the efficiency of XG as a hydraulic control barrier. Further studies should be conducted to verify this behavior.

4.2 Potential and challenges for bio-based hydrogel grouting in geotechnical engineering

One of the major potential challenges with the use of biopolymers for grouting is the economic feasibility. Biopolymers are significantly more expensive than conventional permeable grout materials, such as cement. In particular, the price of one metric ton of XG is approximately USD 2,000 (price taken from Alibaba.com) while one metric ton of cement costed USD 123 in the USA in 2019 (USGS 2020).

Although the material price of biopolymers is higher than that of conventional grouting materials (e.g., cement), significantly lower concentrations of biopolymers are required in geotechnical engineering applications (i.e., 0.5-5% concentrations by mass), while Portland cement is typically applied with 10% or higher contents (i.e., cement to soil ratio in mass) when treating sandy soil. Moreover, because biopolymers such as XG exploit their viscous properties to inhibit the movement of water within the soil mass, their effect can be considered nearly immediate unlike materials such as cement, in which continued pumping may be required until setting. For instance, the hydraulic conductivity of 25% Portland cement treated medium sand ($D_{50} \approx 0.7$ mm) after 28 days-curing has shown similar performance with 1.25% (M_{XG}/M_W) XG hydrogel-injected sand in this study (Kumar 2010). With such considerations, the use of biopolymer for grouting application may prove to be a more cost-effective solution.

Additionally, the global capital market of biopolymers is growing and, with an annual growth rate of 17%, is expected to reach USD 10 billion by 2021 (Xia *et al.* 2020). With such an emerging market, it is expected that the production capabilities of biopolymers will continually improve and that their market price will drop.

Another major challenge with the use of biopolymers is the material durability. As an organic polymer, biopolymers may be extremely susceptible to degradation. Therefore, the effects of long-term exposure to internal pore pressures,

time, weather, organisms, and temperature will need to be investigated in future studies.

5. Conclusions

In this study, the injection performance of XG hydrogel in soil for grouting purposes was examined. Linear injection tests verified that the injection capabilities were highly dependent on the XG concentration and the applied injection pressures. It was found that with higher biopolymer concentrations, the viscosity of the XG solution increases, thereby reducing the injection performance of the grout material. However, it was also observed that, owing to the shear thinning properties of XG at higher injection pressures, the effective viscosity within the injection pipes was reduced by up to 5% of the static viscosity at injection pressures above 400 kPa. These results indicate that the injectability of the XG solution can be controlled by maintaining a proper ratio between the XG concentration and the injection pressure.

In the case of XG injection into a particulate media, it was observed that the pore size affected the maximum groutable volume. The XG solution was still groutable with the smaller pore spaces, but the overall efficiency was reduced because the highly viscous XG solution created larger dragging forces between the particle surfaces and XG solution.

With regards to the effectiveness of XG injection as a grout material for hydraulic conductivity reduction, it was observed that the injection method achieved similar levels of hydraulic conductivity reduction as those seen in previous studies. Along with the fact that XG injection shows immediate reductions in the hydraulic conductivity, the prospect of using such biopolymers for various grouting purposes looks very promising.

Acknowledgments

The research described in this paper was financially supported by a grant from the Water Management Research Program funded by the Ministry of Land, Infrastructure, and Transport (MOLIT) of the Korean government (21AWMP-B114119-06); and the first author is supported by the Innovated Talent Education Program for Smart City from MOLIT. Also this work was supported by the National Research Foundation of Korea (NRF) grant funded by the Korean government (MSIT) (No. 2017R1A5A1014883).

References

Akbulut, S. and Saglamer, A. (2002), "Estimating the groutability of granular soils: A new approach", *Tunn. Undergr. Sp. Tech.*, **17**(4), 371-380. https://doi.org/10.1016/S0886-7798(02)00040-8.

ASTM (2019), D2434-19 Standard Test Method for Permeability of Granular Soils (Constant Head), ASTM International, West Conshohocken, Pennsylvania, U.S.A.

Bell, F. (1993), *Engineering Treatment of Soils*, CRC Press, Florida, U.S.A.

Benhelal, E., Zahedi, G., Shamsaei, E. and Bahadori, A. (2013), "Global strategies and potentials to curb CO2 emissions in cement industry", *J. Clean. Prod.*, **51** 142-161. https://doi.org/10.1016/j.jclepro.2012.10.049.

Bouazza, A., Gates, W. and Ranjith, P. (2009), "Hydraulic conductivity of biopolymer-treated silty sand", *Géotechnique*. **59**(1), 71-72. https://doi.org/10.1680/geot.2007.00137.

Burwell, E. (1958), "Cement and clay grouting of foundations: Practice of the corps of engineers", *J. Soil Mech. Found. Div.* **84**(1), 1-22. https://doi.org/10.1061/JSFEAQ.0000099.

Cabalar, A.F., Wiszniewski, M. and Skutnik, Z. (2017), "Effects of xanthan gum biopolymer on the permeability, odometer, unconfined compressive and triaxial shear behavior of a sand", *Soil Mech. Found. Eng.*, **54**(5), 356-361. https://doi.org/10.1007/s11204-017-9481-1.

Casas, J.A., Santos, V.E. and García-Ochoa, F. (2000), "Xanthan gum production under several operational conditions: Molecular structure and rheological properties", *Enzyme Microb. Tech.*, **26**(2-4), 282-291. https://doi.org/10.1016/S0141-0229(99)00160-X.

Chang, I. and Cho, G.C. (2012), "Strengthening of Korean residual soil with β-1,3/1,6-glucan biopolymer", *Constr. Build. Mater.*, **30**, 30-35. https://doi.org/10.1016/j.conbuildmat.2011.11.030.

Chang, I., Im, J. and Cho, G.C. (2016), "Geotechnical engineering behaviors of gellan gum biopolymer treated sand", *Can. Geotech. J.*, **53**(10), 1658-1670. https://doi.org/10.1139/cgj-2015-0475.

Chang, I., Im, J. and Cho, G.C. (2016), "Introduction of microbial biopolymers in soil treatment for future environmentally-friendly and sustainable geotechnical engineering", *Sustainability*, **8**(3), 251. https://doi.org/10.3390/su8030251.

Chang, I., Im, J., Prasidhi, A.K. and Cho, G.C. (2015), "Effects of xanthan gum biopolymer on soil strengthening", *Constr. Build. Mater.*, **74**, 65-72. https://doi.org/10.1016/j.conbuildmat.2014.10.026.

Chang, I., Lee, M. and Cho, G.C. (2019), "Global CO_2 emission-related geotechnical engineering hazards and the mission for sustainable geotechnical engineering", *Energies*. **12**(13), 2567. https://doi.org/10.3390/en12132567.

Chang, I., Lee, M., Tran, A.T.P., Lee, S., Kwon, Y.M., Im, J. and Cho, G.C. (2020), "Review on biopolymer-based soil treatment (BPST) technology in geotechnical engineering practices", *Transport. Geotech.*, **24**, 100385.

Chang, I., Prasidhi, A.K., Im, J. and Cho, G.C. (2015), "Soil strengthening using thermo-gelation biopolymers", *Constr. Build. Mater.*, **77**, 430-438. https://doi.org/10.1016/j.conbuildmat.2014.12.116.

Chang, I., Prasidhi, A.K., Im, J., Shin, H.D. and Cho, G.C. (2015), "Soil treatment using microbial biopolymers for anti-desertification purposes", *Geoderma*, **253-254**, 39-47. https://doi.org/10.1016/j.geoderma.2015.04.006.

Choi, S.G., Chang, I., Lee, M., Lee, J.H., Han, J.T. and Kwon, T.H. (2020), "Review on geotechnical engineering properties of sands treated by microbially induced calcium carbonate precipitation (MICP) and biopolymers", *Constr. Build. Mater.*, **246**, 118415. https://doi.org/10.1016/j.conbuildmat.2020.118415.

DeJong, J.T., Mortensen, B.M., Martinez, B.C. and Nelson, D.C. (2010), "Bio-mediated soil improvement", *Ecol. Eng.*, **36**(2), 197-210. https://doi.org/10.1016/j.ecoleng.2008.12.029.

Eklund, D. and Stille, H. (2008), "Penetrability due to filtration tendency of cement-based grouts", *Tunn. Undergr. Sp. Tech.*, **23**(4), 389-398. https://doi.org/10.1016/j.tust.2007.06.011.

García-Ochoa, F., Santos, V.E., Casas, J.A. and Gómez, E. (2000), "Xanthan gum: production, recovery, and properties",

Biotechnol. *Adv*., **18**(7), 549-579. https://doi.org/10.1016/S0734-9750(00)00050-1.

Gupta, S. and Larson, W. (1979), "A model for predicting packing density of soils using particle-size distribution", *Soil Sci*. *Soc*. *Am*. *J*., **43**(4), 758-764. https://doi.org/10.2136/sssaj1979.03615995004300040028x.

Ham, S.M., Chang, I., Noh, D.H., Kwon, T.H. and Muhunthan, B. (2018), "Improvement of surface erosion resistance of sand by microbial biopolymer formation", *J. Geotech*. *Geoenviron*. *Eng*., **144**(7), 06018004. https://doi.org/10.1061/(ASCE)GT.1943-5606.0001900.

Jeon, M.K., Kwon, T.H., Park, J.S. and Shin, J.H. (2017), "In situ viscoelastic properties of insoluble and porous polysaccharide biopolymer dextran produced by Leuconostoc mesenteroides using particle-tracking microrheology", *Geomech*. *Eng*., **12**(5), 849-862. https://doi.org/10.12989/gae.2017.12.5.849.

Jin, H., Ryu, B. and Lee, J. (2016), "Development and assessment of laboratory testing apparatus on grouting injection performance", *J*. *Kor*. *Geoenviron*. *Soc*., **17**(10), 23-31. https://doi.org/10.14481/jkges.2016.17.10.23.

Kim, Y.M., Park, T. and Kwon, T.H. (2019), "Engineered bioclogging in coarse sands by using fermentation-based bacterial biopolymer formation", *Geomech*. *Eng*., **17**(5), 485-496. https://doi.org/10.12989/gae.2019.17.5.485.

Ko, D. and Kang, J. (2018), "Experimental studies on the stability assessment of a levee using reinforced soil based on a biopolymer", *Water*, **10**(8), 1059. https://doi.org/10.3390/w10081059.

Kumar, S. (2010), "A study on the engineering behaviour of grouted loose sandy soils", Ph.D. Dissertation, Cochin University of Science, Kochi, India

Kwon, Y.M., Ham, S.M., Kwon, T.H., Cho, G.C. and Chang, I. (2020), "Surface-erosion behaviour of biopolymer-treated soils assessed by EFA", *Géotechnique Lett*., **10**(2), 1-7. https://doi.org/10.1680/jgele.19.00106.

Larson, S., Ballard, J., Griggs, C., Newman, J.K. and Nestler, C. (2010). "An innovative non-ptroleum Rhizobium Tropici biopolymer salt for soil stabilization", *Proceedings of the ASME 2010 International Mechanical Engineering Congress and Exposition*, Vancouver, Canada.

Lee, J., Frost, D., Lee, J. and Dremin, A. (1995), "Propagation of nitromethane detonations in porous media", *Shock Waves*, **5**(1-2), 115-119. https://doi.org/10.1007/BF02425043.

Lee, M., Im, J., Cho, G.C., Ryu, H.H. and Chang, I. (2021), "Interfacial shearing behavior along Xanthan gum biopolymer-treated sand and solid interfaces and its meaning in geotechnical engineering aspects", *Appl*. *Sci*., **11**(1), 139. https://doi.org/10.3390/app11010139.

Lee, S., Im, J., Cho, G.C. and Chang, I. (2019), "Laboratory triaxial test behavior of xanthan gum biopolymer-treated sands", *Geomech*. *Eng*., **17**(5), 445-452. https://doi.org/10.12989/gae.2019.17.5.445.

Liu, Z. and Yao, P. (2015), "Injectable shear-thinning xanthan gum hydrogel reinforced by mussel-inspired secondary crosslinking", *RSC Adv*., **5**(125), 103292-103301. https://doi.org/10.1039/C5RA17246B.

Noh, D.H., Ajo-Franklin, J.B., Kwon, T.H. and Muhunthan, B. (2016), "P and S wave responses of bacterial biopolymer formation in unconsolidated porous media", *J. Geophys*. *Res*. *Biogeosci*., **121**(4), 1158-1177. https://doi.org/10.1002/2015JG003118.

Qureshi, M.U., Chang, I. and Al-Sadarani, K. (2017), "Strength and durability characteristics of biopolymer-treated desert sand", *Geomech*. *Eng*., **12**(5), 785-801. https://doi.org/10.12989/gae.2017.12.5.785.

Santagata, M. and Santagata, E. (2003), "Experimental investigation of factors affecting the injectability of microcement grouts", *Proceedings of the 3rd International Conference on Grouting and Ground Treatment*, New Orleans, Louisiana, U.S.A., Febrauary.

Santamarina, J.C., Klein, K.A. and Fam, M.A. (2001), *Soils and Waves*, John Wiley & Sons, Chichester, New York, U.S.A.

Soldo, A., Miletić, M. and Auad, M.L. (2020), "Biopolymers as a sustainable solution for the enhancement of soil mechanical properties", *Sci*. *Rep*., **10**(1), 267. https://doi.org/10.1038/s41598-019-57135-x.

Sworn, G. (2021), *Chapter 27 - Xanthan Fum*, in *Handbook of Hydrocolloids*, Woodhead Publishing

Tran, A.T.P. (2019), "Characterization of biopolymer-treated soils considering soil-water-hydrogel Interaction", KAIST, Daejeon, Korea.

Tran, A.T.P., Chang, I. and Cho, G.C. (2019), "Soil water retention and vegetation survivabiity improvement using microbial biopolymers in drylands", *Geomech. Eng.*, **17**(5), 475-483. https://doi.org/10.12989/gae.2019.17.5.475.

USGS (2020), *Mineral Commodity Summaries 2020*, U.S. Geological Survey: National Minerals Information Center, Reston, Virginia, U.S.A.

Whiffin, V.S., van Paassen, L.A. and Harkes, M.P. (2007), "Microbial carbonate precipitation as a soil improvement technique", *Geomicrobiol*. *J*., **24**(5), 417-423. https://doi.org/10.1080/01490450701436505.

Xia, S., Zhang, L., Davletshin, A., Li, Z., You, J. and Tan, S. (2020), "Application of polysaccharide biopolymer in petroleum recovery", *Polymers*, **12**(9), 1860. https://doi.org/10.3390/polym12091860.

Yoon, J. and El Mohtar, C.S. (2014), "Groutability of granular soils using bentonite grout based on filtration model", *Transport*. *Porous Med*., **102**(3), 365-385. https://doi.org/10.1007/s11242-014-0279-6.

Zhong, L., Oostrom, M., Truex, M.J., Vermeul, V.R. and Szecsody, J.E. (2013), "Rheological behavior of xanthan gum solution related to shear thinning fluid delivery for subsurface remediation", *J. Hazard*. *Mater*., **244** 160-170. https://doi.org/10.1016/j.jhazmat.2012.11.028.

IC